Hindawi
Advances in Materials Science and Engineering
Volume 2019, Article ID 7974628, 11 pages
https://doi.org/10.1155/2019/7974628

Research Article

Coal Reservoir Characterization in a Tectonic Setting and the Effects of Tectonism on the Coalbed Methane (CBM) Content

Zhenni Ye,[1,2] Enke Hou,[1] Zhonghui Duan,[2,3] and Zengjiang Li[4]

[1] *College of Geology and Environment, Xi'an University of Science and Technology, Xi' an 710054, China*
[2] *Key Laboratory of Coal Resources Exploration and Comprehensive Utilization, Ministry of Land and Resources, Xi'an 710026, Shaanxi, China*
[3] *Shaanxi Coal Geology Group Co., Ltd, Xi'an 710026, Shaanxi, China*
[4] *College of Medical Technology, Xi'an Medical University, Xi'an 710021, China*

Correspondence should be addressed to Zhenni Ye; 58334686@qq.com

Received 9 October 2018; Revised 31 December 2018; Accepted 9 January 2019; Published 13 February 2019

Academic Editor: Carlos R. Rambo

Copyright © 2019 Zhenni Ye et al. This is an open access article distributed under the Creative Commons Attribution License, which permits unrestricted use, distribution, and reproduction in any medium, provided the original work is properly cited.

Research on the relationships among tectonics, micropores, microfractures, and coalbed methane (CBM) content is important for the optimal selection of CBM production areas. In this study, micropore-microfracture structural parameters of coal samples from the Guojiahe coalfield are determined through the use of X-ray photography, an image recognition algorithm, and a liquid nitrogen adsorption method. The relationship between the micropore-microfracture characteristics of the reservoir and the gas content is quantitatively assessed using the Grassberger and Procaccia (GP) algorithm to calculate the correlation dimension of the parameters. Micropore-microfracture development varies in different tectonic zones. Additionally, the CBM content varies according to the characteristic parameters of hysteresis loops and the pore diameter. The correlation dimension is an effective indicator of the nonlinear relationship between reservoir micropore-microfracture characteristics and the gas content.

1. Introduction

Various geological factors, including tectonics, coal reservoir properties, and coal seam thickness, can strongly impact enhanced coalbed methane (CBM) extraction [1]. In particular, coal reservoirs that have experienced multistage tectonic events show obvious property differences in terms of pore-fracture systems [2–4]. Thus, studies of the coal reservoir microfeatures associated with tectonics-induced effects on the CBM content could be conducted to optimize CBM extraction projects. Currently published results mainly focus on the structural characteristics of micropores and microfractures for use in the evaluation of the CBM exploitation potential [5]. Furthermore, previous publications have largely focused on the pore characteristics of reservoirs and the reservoir structure without considering the connection between variations in pore characteristics and tectonics [6, 7]. Other studies have focused on CBM accumulation only from a tectonic perspective. Notably, previous studies have found that CBM is enriched above the neutral planes of synclines and below those of anticlines, due to compression forces [8]. Additionally, extensional faults provide channels for gas emissions, and tectonism is the main factor that causes variations in the pore-fracture structures of coal reservoirs and results in nonuniform distributions of CBM. Specifically, the pore-fracture features vary based on structural forms and affect gas migration, accumulation, and preservation. Thus, it is worth considering pore-fracture characteristics in different types of tectonic zones and the associated effects on the gas content.

Coal reservoirs comprise pores and fractures [9], which can be subdivided into macrofractures, microfractures, macropores, and micropores according to pore-fracture size [10–12]. The hybrid methods used to study reservoirs include liquid nitrogen adsorption or carbon dioxide adsorption [13, 14], mercury injection experiments [15], scanning electron microscopy (SEM) [16], low-field nuclear magnetic resonance (NMR) [17–19]. Among these, experiments involving liquid nitrogen adsorption and carbon dioxide adsorption can obtain estimates of different pore sizes and percentages. Adsorption pores strongly affect the gas storage capacity of coals through the pore structure system and gas diffusion through the fracture structure system. Therefore, these results provide important guidance for gas extraction from coal seams and for gas-related hazard prevention during coal mining. SEM images can show pores or the fractures on the surface of coal samples. The internal fracture characterization of a coal mass can produce an estimate of the 3D structure [20, 21], which can be quantitatively analyzed by means of X-ray penetration using digital radiography (DR) systems [20]. Yao et al. [17] presented a new approach of combining NMR and X-ray computed tomography to quantitatively describe the types of size distribution and spatial arrangement of pores and fractures.

In this paper, liquid nitrogen adsorption and a DR system are combined with an X-ray image recognition algorithm to identify the micropore and microfracture structural characteristics of coal reservoir samples collected from geological structures. Based on the Grassberger and Procaccia (GP) algorithm [22], various micropore and microfracture system parameters and CBM contents are calculated to determine the micropore and microfracture structure of a coal reservoir, as well as the associated effects of this structure on the gas content of the reservoir.

2. Regional Geotectonic Characteristics

In this paper, the Guojiahe coalfield in the Yonglong mining area, China, is selected as the case study. The coalfield is located in the western Miaobin Depression and north of the Weibei Flexure Belt tectonic unit (Figure 1). The regional strata consist of the Tongchuan, Fuxian, Yanan, Zhiluo, Anding, Yijun, Luohe, and Huachi Formations, as well as Neogene, Middle-Late Pleistocene, and Holocene units, in chronological order. The Middle Jurassic Yanan Formation includes coal-bearing strata, and the thickness of the main No. 3 coal seam ranges from 0.55 m to 26.83 m, with an average thickness of 11.88 m in the area.

The Yanan Coal Formation was formed by the Indosinian Movement and the first phase of the Yanshan Movement [23]. The folded strata dip gently to the NW-NNW and strike NE-NEE. These characteristics are controlled by the N-E (35°) paleostructure created by the Indosinian Movement [24, 25]. The Liangting anticline extends inward to the coalfield. The anticline axis not only resulted in the nondeposition of the Yanan Formation but also in thin coal deposits, with a thickness of 2 to 5 m. However, the Yanan Formation exhibits good coal thickness of 15.2 to 27.9 m along the axis of the Caizigou-Zhangba syncline (Figure 1). Thus, the distribution of the coal seam thickness is controlled by the paleostructure and gradually thins toward the anticline and thickens toward the syncline.

3. Coal Reservoir Characterization under the Tectonic Setting

3.1. Fracture Identification Method with the DR System. DR is an effective method of identifying the microfeatures of coal samples [20]. This method can quantify fractures by projecting a three-dimensional fracture network onto a plane. In this paper, the microfeatures of twenty-five coal samples from eleven coal sampling locations are studied using an Angell-1500R DR system (Figure 2). Two to three samples were taken at each location, and twenty-five samples were taken from the different tectonic zones of the Guojiahe coalfield in China, as shown in Figure 3. The system parameters of the DR system are presented in Table 1.

3.2. Fracture Characterization of Coal Samples. Quantitative analysis is the basic research method for determining the gas distribution in fractured coal. The fractal dimension [26], joint roughness coefficient (JRC) [27], and rock mass system (RMS) [28] methods have been commonly used to measure the macrofracture and microfracture characteristics of a coal-rock mass. Image processing software and the Kirsch operator image analysis method are used in this study to identify fracture characteristics and express them as parameter C_i. The equation for C_i is as follows:

$$C_i = \frac{h_{\max}}{l}, \tag{1}$$

where $h_{\max}$ (mm) is the maximum gap between tectonic fractures in a plane projection, l (mm) is the length of tectonic fractures in a plane projection, and i is the number of fractures.

Image progressing software (Image-Pro) and the Kirsch operator image analysis method are used to detect the edges and identify the parameters of microfractures obtained by X-ray photography (Figure 4). Then, the microfracture parameter C_i is calculated.

The structure of microfractures obtained by the DR system appears as veins or clusters (Figure 5). Among the twenty-five coal samples, five samples from the points GJH3-X2, GJH3-01, and GJH3-02 exhibited no structural fractures. Additionally, three samples from points GJH3-03 and GJH3-04 had fracture lengths shorter than 20 mm and a maximum gap of less than 0.5 mm and are not listed because fractures with a reasonable size provide seepage channels rather than emission channels. Then, based on the proportion of fractures longer than 20 mm and wider than 0.5 mm, six coal samples out of the remaining seventeen were selected as representative samples for each point to calculate the fracture parameter. The maximum gap ranged from 0.54 to 6.94 mm, the length ranged from 23.16 to 130.1 mm, and the linear density ranged from 8.28 to 23.7 fractures per meter. Because tectonic fractures of reasonable size are the main channels for CBM migration [29], the maximum projected area of fractures was used to calculate C_i.

A detailed analysis was performed based on the Kirsch method, and the pixel dimension of images of representative samples is shown in Figure 5. The relationships between microfracture parameters and tectonic zones indicate that microfracture characteristics vary in different zones. Specifically, small C_i values reflect a longer projected fracture length and a low level of microfracture development.

The C_i values of GJH3-F1 to GJH3-F4 vary from 0.034 to 0.059, and the fracture density ranges from 16.93 to 23.7 in the fault area, as shown in Figure 6. These values indicate that faults have a considerable influence on the density and

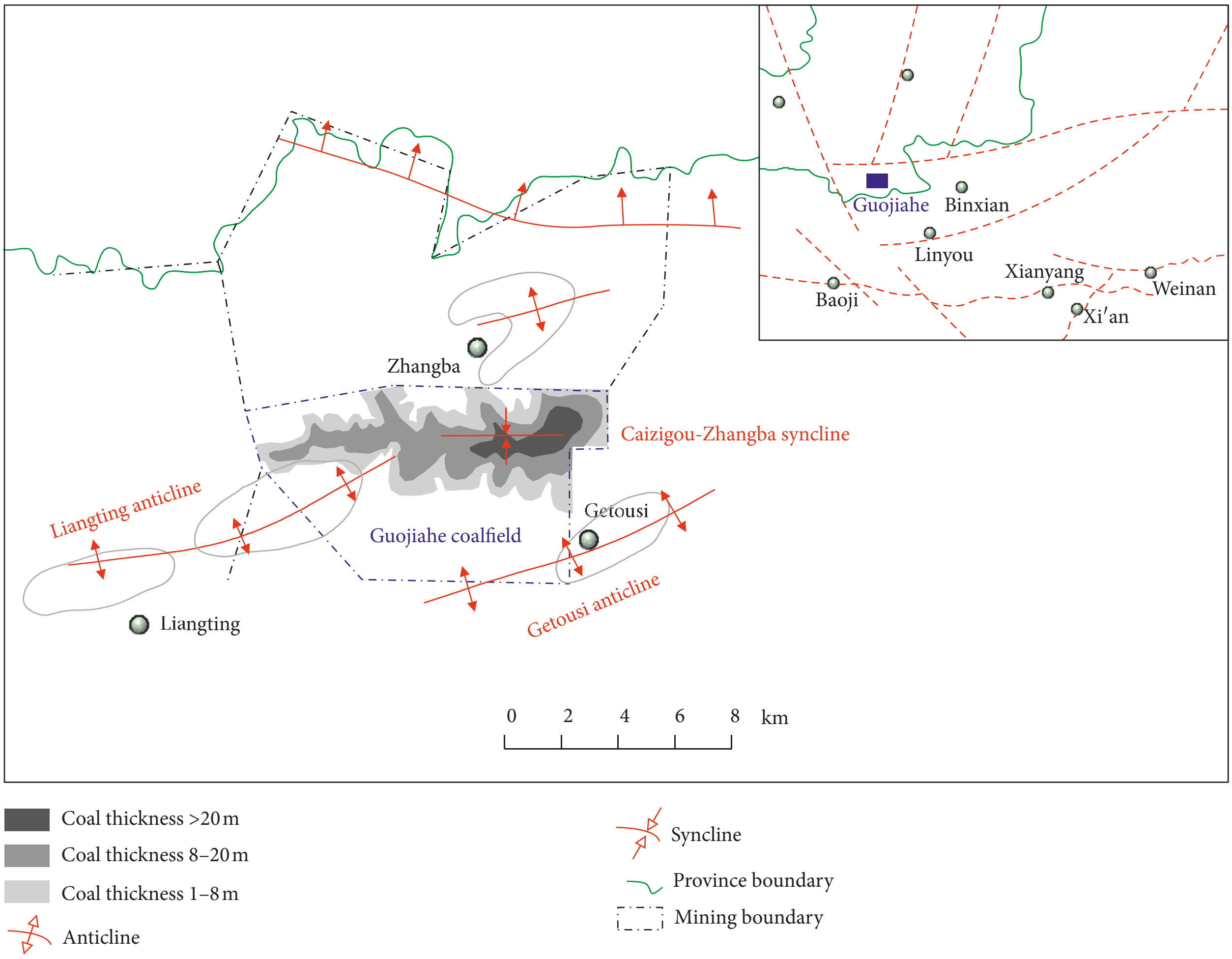

FIGURE 1: Tectonic features of Guojiahe coalfield.

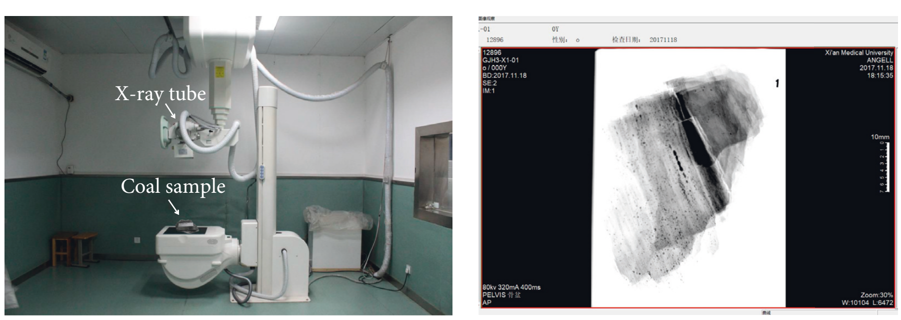

(a) (b)

FIGURE 2: Digital radiography system and X-ray image of a coal sample: (a) digital radiography equipment and system; (b) X-ray image of the coal sample and image window.

development of microfractures. The C_i values differ in different tectonic zones, and the B1 anticline has a notable influence on coal microfracture development. The fracture density is relatively small near the X1 syncline and B1 anticline, which indicates that tectonic movement may have little effect on the microfeatures of coal samples in syncline and anticline zones. In conclusion, the development degree of microfractures varies based on the tectonic zone.

3.3. Pore Characterization of Coal Samples. The majority of CBM accumulation occurs in coal pores, and the pore structure parameters are key indicators that can be used to evaluate coal seam adsorption. Specifically, liquid nitrogen experiments can be performed to investigate coal pore characteristics [14]. The method is suitable for pore diameters ranging from 1 to 20 nm, and this method has a wider measuring range than the method based on carbon

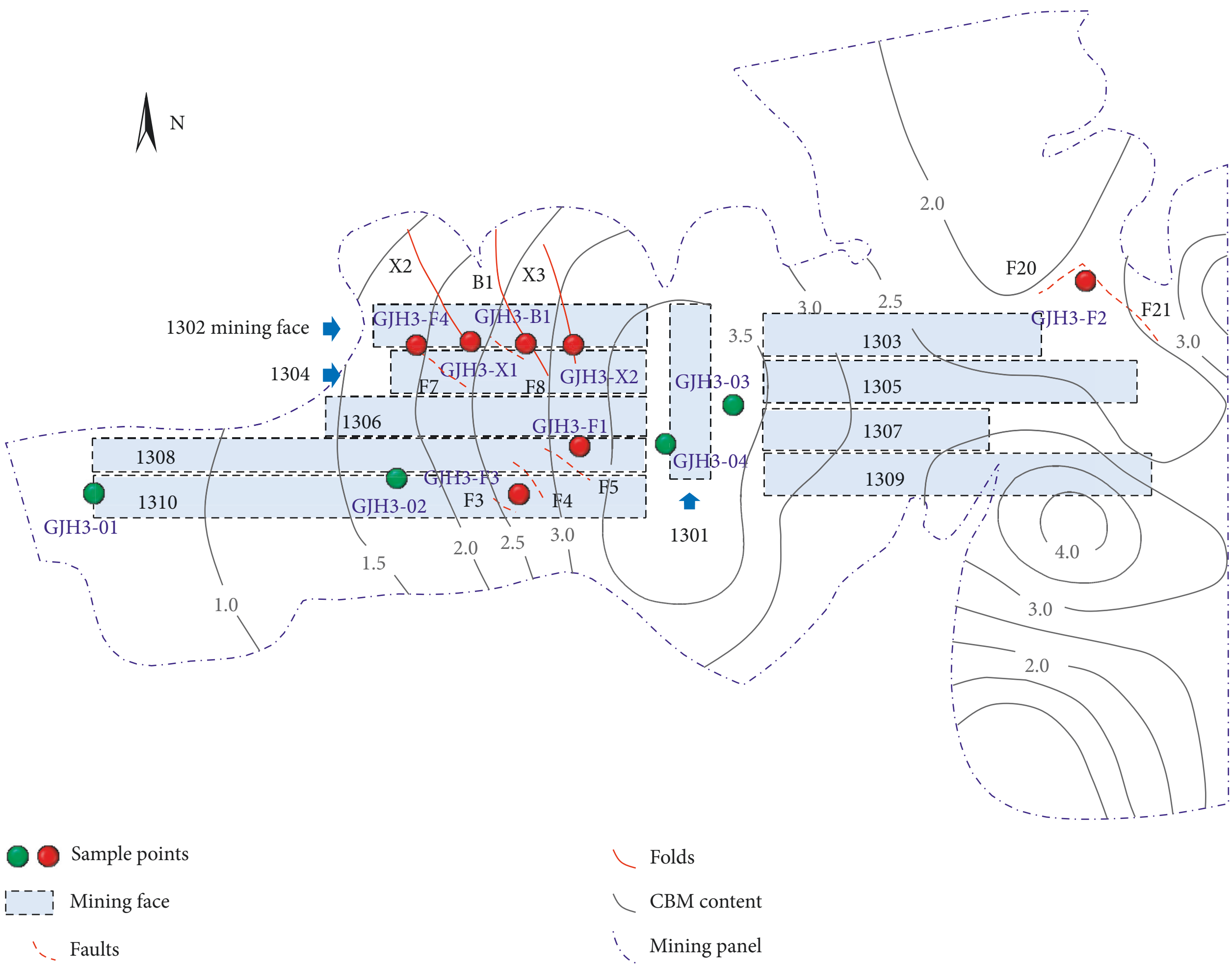

FIGURE 3: Coal sampling points and mining face sites.

TABLE 1: Sampling locations and voltage parameters of the DR system.

Number	Location	System parameters		
		Voltage (kVp)	Electric current (mA)	Attack time (ms)
GJH3-X1	17 m from X2 syncline	80	320	110
GJH3-X2	13.2 m from X3 syncline	84	320	110
GJH3-B1	4.3 m from B1 anticline	80	320	110
GJH3-F1	149 m from F5 fault	78	320	110
GJH3-F2	51 m from F21 fault	78	320	110
GJH3-F3	92.5 m from F3 fault	82	320	110
GJH3-F4	25 m from F7 fault	83	320	110
GJH3-01	Cutting hole of 1308 coal mining face	79	320	110
GJH3-02	High-position alley of 1308 coal mining face	78	320	110
GJH3-03	Auxiliary transport alleys of eastern I panel	80	320	125
GJH3-04	Auxiliary transport alleys of western I panel	80	320	110

dioxide. ASAP JW-BK122 W is used to obtain the relative pressure and adsorption curve under isothermal conditions and classify the adsorption-desorption isotherms. The slope K_i and length L_i of a straight line passing through an initial point $(P'/P_0, V')$ and end point $(P^*/P_0, V^*)$ of an isotherm can be calculated as follows:

$$K_i = \frac{V^* - V'}{(P^*/P_0) - (P'/P_0)},$$
$$L_i = \sqrt{\left(\left(\frac{P^*}{P_0}\right) - \left(\frac{P'}{P_0}\right)\right)^2 + (V^* - V')^2}, \tag{2}$$

where K_i represents the adsorption/desorption value ($\Delta cm^3/g$) associated with a relative pressure change during the capillary and pore condensation process. L_i represents the amount of condensation from capillary pores relative to that from all pores. The adsorption volume associated with a relative pressure depends on the minimum pore size at the

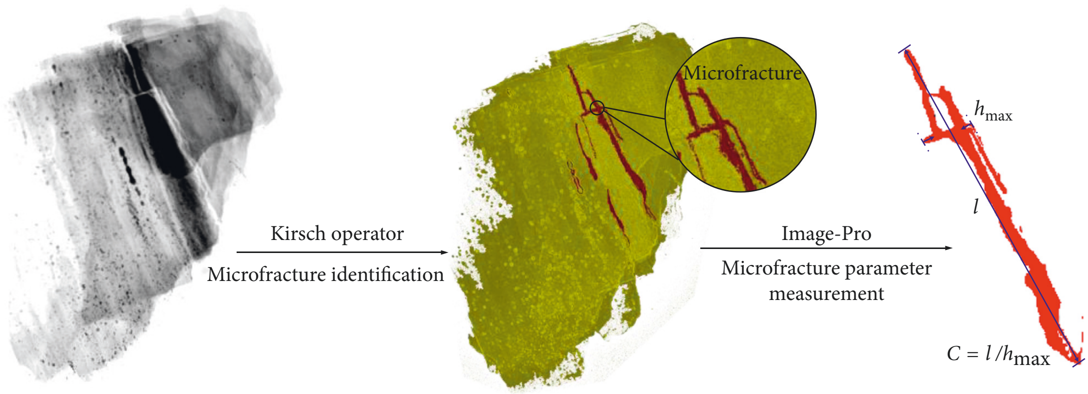

Figure 4: Microfracture parameter identification for coal specimens based on an X-ray image.

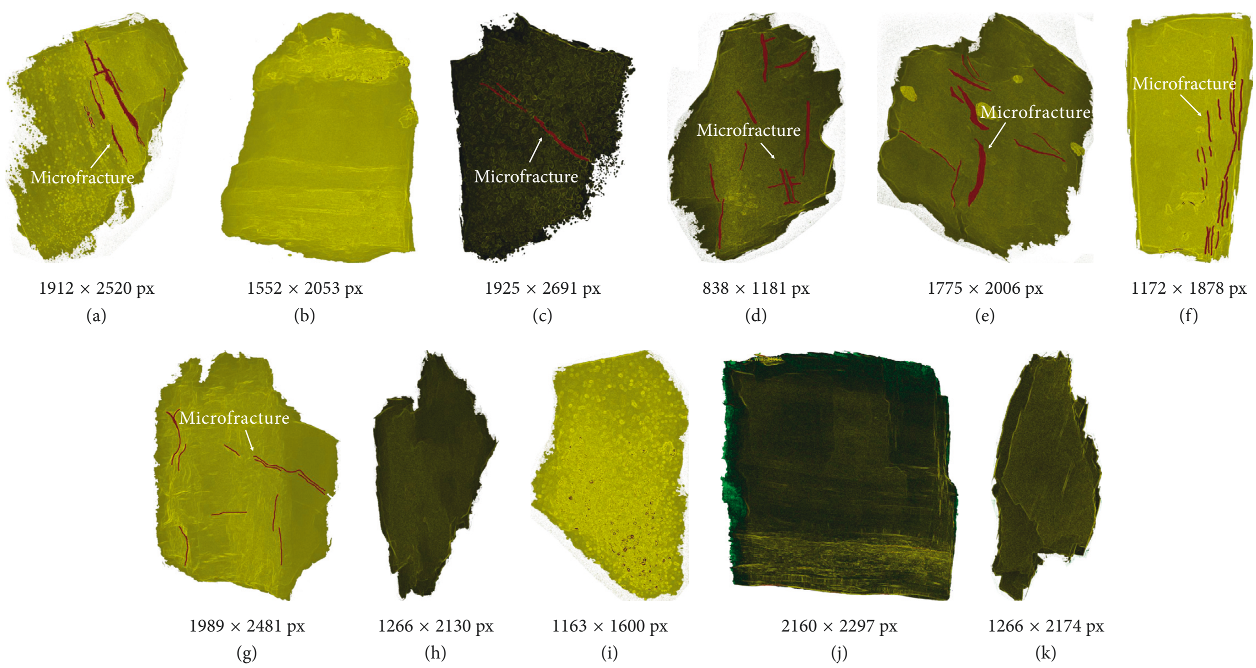

Figure 5: Analysis of the microfractures in X-ray images of coal specimens based on the Kirsch algorithm: (a) GJH3-X1; (b) GJH3-X2; (c) GJH3-B1; (d) GJH3-F1; (e) GJH3-F2; (f) GJH3-F3; (g) GJH3-F4; (h) GJH3-01; (i) GJH3-02; (j) GJH3-03; (k) GJH3-04.

initial point. The length of the process depends on the pore sizes and distribution of pores.

Liquid nitrogen experiments were conducted on seven samples from the syncline, anticline, and fault areas, and 7 isothermal curves with clear hysteresis loops related to the pore shape and size were obtained. Thus, the pore shape, diameter, and distribution were determined by analyzing the hysteresis loop features and calculating the proportion of different pore sizes.

Figure 7 shows the hysteresis loops in different tectonic zones, and the feature parameters K_i and L_i are calculated based on the above equation. The calculation results are shown in Table 2. The hysteresis loops are classified into three types based on their isotherm features. The first type includes large closed loops with initial points at relative pressures of 0.4 to 0.42 and K_i values from 4.35 to 6.94 (Figures 7(a) and 7(b)). This type of loop is observed for syncline samples. The second type includes small closed loops with initial points at a relative pressure of 0.49 and small K_i values. This type of loop is associated with anticline samples. The third type of loop exhibits start points at a relative pressure of 0.17, and K_i varies from 3.23 to 14.57. The third type of loop is observed for fault samples. This classification has also been used in previous studies of hysteresis loops for different coal body structures [30–32]. In some cases, isothermal curves may not form closed loops because liquid nitrogen remained in open-ended micropores with a decrease in relative pressure. Thus, it is scientifically reasonable to define a point on the adsorption curve where the adsorption volume is similar to the desorption value at low relative pressure as the initial point of $K_{i.}$

According to the Ходот, В. В. classification, the pores are mainly micropores with diameters of 3.55 nm to 8.99 nm (average of 5.09 nm). The Brunauer–Emmett–Teller (BET)

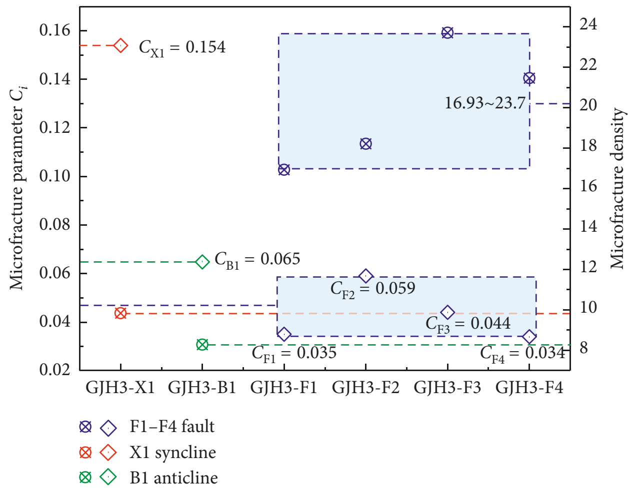

Figure 6: Microfracture parameters of coal specimens in different tectonic zones.

specific surface area ranges from 2.26–15.69 $m^2 \cdot g^{-1}$, with an average of 10.16 $m^2 \cdot g^{-1}$. The Barrett–Joyner–Halenda (BJH) pore capacity ranges from 0.00475 to 0.02122 $cm^3 \cdot g^{-1}$, with an average of 0.0101 $cm^3 \cdot g^{-1}$. The pore diameters of coal samples in syncline and anticline areas exhibited a small difference, but those in the fault area were considerably different. Specifically, the pore diameters of coal samples from the fault zone were larger than those from syncline or anticline areas.

The proportions of different pore sizes in different tectonic samples are shown in Table 3. The pore capacity and diameter class of greater than 2 nm is abundant in the fault zone area but not in the syncline and anticline areas. The pore size distribution may be related to the tectonic forces in the area because such forces may change the pore and fracture structures by destroying primary pores and developing apertures, mesopores, and macropores. In conclusion, different tectonic zones influence the pore diameter and distribution in different ways.

4. Tectonic Effects on the Coalbed Methane Content

4.1. Correlation Dimension Calculation with the GP Algorithm. The GP algorithm is one effective method of calculating the correlation dimension of chaotic time series [33]. Correlation dimension analysis is an important branch of fractal theory, and this dimension is used as an indicator to evaluate complex trends in data. The microfracture parameters, pore characteristic parameters, and gas content were investigated based on a series of i collected samples:

$$N = [n_1,\ n_2,\ n_3 \cdots n_i]. \tag{3}$$

Selecting a subset of values from the above equation yields an m-dimensional phase space N_1:

$$N_1 = [n_1,\ n_2,\ n_3 \cdots n_m]. \tag{4}$$

The number of values in the m-dimensional phase space is $n - m + 1$. Thus, the correlation function is as follows:

$$C(r) = \frac{1}{N^2} \sum_{i=1}^{N} \sum_{j=1}^{N} H\left(r - \left|N_i - N_j\right|\right). \tag{5}$$

In equation (5), $H(x)$ represents the Heaviside function:

$$H(x) = \begin{cases} 0, & x \le 0, \\ 1, & x > 0, \end{cases} \tag{6}$$

where r has a given value of $r = kr_0$. In this relation, k is a segment of radius r, and r is equal to 8 in this paper. Additionally, the minimum embedding dimension is 1, the maximum embedding dimension is 10, and the delay time is 2. The correlation dimension is the slope of the straight line fit to $\ln(r)$ and $\ln C(r)$ plotted in log-log coordinates:

$$D = \frac{\ln C(r)}{\ln(r)}. \tag{7}$$

4.2. CBM Content Analysis in Different Types of Tectonic Zones. Structural geologic factors, such as coal thickness, burial depth, and fault distribution, are important factors influencing CBM accumulation [34–36]. Coal microfeature evolution is influenced by multiphase tectonic activity, which can lead to gas migration, diffusion, and concentration variations. In this paper, panel I of Guojiahe coalfield is used as an engineering example, and the micropore-microfracture parameters and gas content are analyzed. Based on the GP algorithm, the correlation dimension is calculated to quantitatively analyze the relationship between tectonics and the gas content. The results of this analysis can be used to optimize CBM production in different zones.

Coal microfeatures are related to the gas content. Based on previous experimental data collected from a borehole during the exploitation period, the contours of the CBM content are illustrated in Figure 3. Microfeature data obtained using the DR system and via liquid nitrogen experiments and the gas contents of coal samples are listed in Table 4. Gaussian fitting is an effective method of analyzing the relationships among these data, and the fitting results are shown in Figure 8.

The microfracture parameter C_i reflects the development of coal fractures, which influence the migration and emission of CBM. Specifically, gas migrates and spreads along coal fractures, and this process often decreases the gas content. The relationship between the microfracture parameter C_i and the gas content was analyzed based on Gaussian fitting, and the results are shown in Figure 8(a). C_i reaches a peak at 0.154, when the gas content is 2.365 m^3/t, and the average value of C_i is 0.055. When the gas content is greater than 2.52 m^3/t, C_i remains small. This result suggests that the tectonic fractures in the studied plane projection are relatively long, and long fractures are generally associated with low gas contents. Figure 8(a) shows that the gas content is high in more than half of the samples, but the C_i values are less than 0.06. The Gaussian curve exhibits a small width and high peak, which indicates that data are centrally distributed and that C_i is highly correlated with the gas content of samples from different tectonic zones.

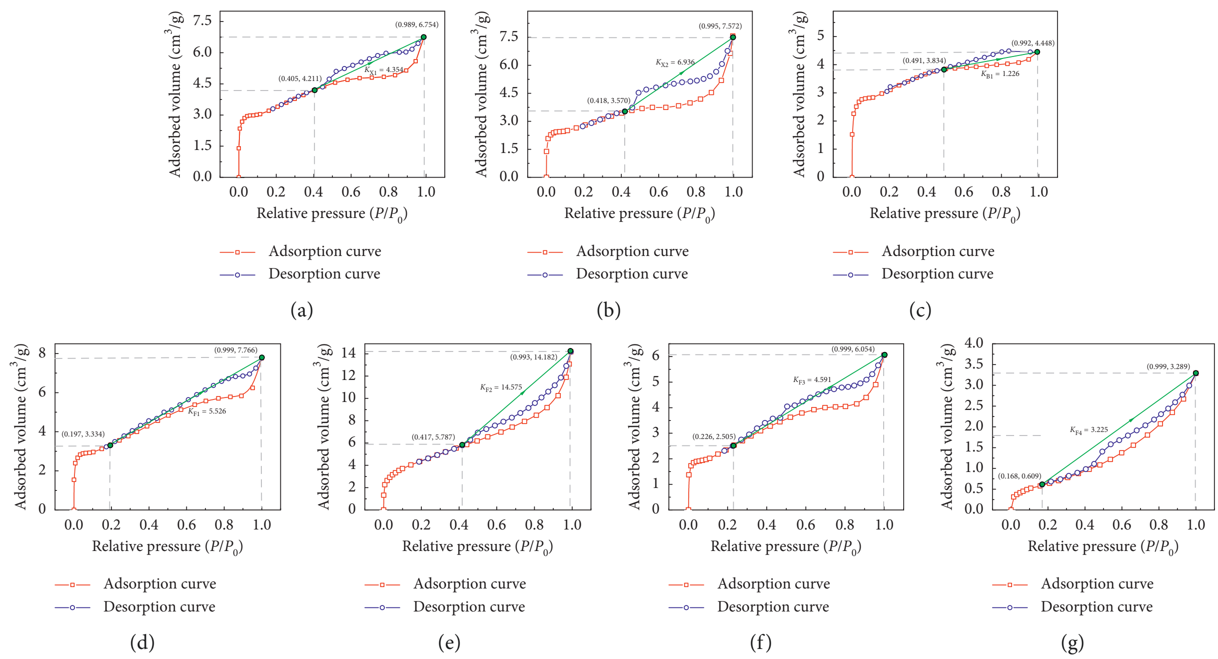

Figure 7: N_2 adsorption/desorption isotherms in tectonic zones: (a) GJH3-X1; (b) GJH3-X2; (c) GJH3-B1; (d) GJH3-F1; (e) GJH3-F2; (f) GJH3-F3; (g) GJH3-F4.

Table 2: Parameter variations based on the hysteresis loops.

	GJH3-X1	GJH3-X2	GJH3-B1	GJH3-F1	GJH3-F2	GJH3-F3	GJH3-F4
K_i	4.354	6.936	1.226	5.526	14.575	4.591	3.225
L_i	2.609	4.043	0.792	4.504	8.415	3.632	2.806

Table 3: Analysis results for the specific surface area and low-temperature nitrogen adsorption.

Number	Average diameter of adsorption pore (nm)	BET specific surface area ($m^2 \cdot g^{-1}$)	BJH pore capacity ($cm^3 \cdot g^{-1}$)	The proportions of different pore sizes in %*		
				<2 nm	2–10 nm	>10 nm
GJH3-X1	3.55269	11.76367	0.00896	54.07	38.30	7.63
GJH3-X2	4.83339	9.69391	0.00948	39.27	24.11	36.62
GJH3-B1	3.99535	11.82743	0.00475	65.40	28.31	6.29
GJH3-F1	4.12462	11.65071	0.01100	41.2	41.09	17.71
GJH3-F2	5.59499	15.68541	0.02122	30.13	37.70	32.17
GJH3-F3	4.55398	8.22590	0.00962	22.05	49.57	28.38
GJH3-F4	8.99411	2.26251	0.00569	8.32	57.42	34.26

Note: the letter X in the numbers of coal samples represents the syncline area, B represents the anticline area, and F represents the fault area. *Calculated by pore volume distribution.

Table 4: Gas content and micropore-microfracture parameters in different tectonic zones.

Number	Fracture development (microfracture parameter) C_i	Pore structure characteristics (feature parameters of hysteresis loop) K_i	L_i	Gas content (q_i/$m^3 \cdot t^{-1}$)
GJH3-X1	0.154	4.354	2.609	2.365
GJH3-B1	0.065	1.226	0.792	2.787
GJH3-F1	0.035	5.526	4.504	3.232
GJH3-F2	0.059	14.575	8.415	2.179
GJH3-F3	0.044	4.591	3.632	2.686
GJH3-F4	0.034	3.225	2.806	1.921

The liquid nitrogen hysteresis loops reflect the coal pore shape and pore size distribution, which influence the CBM content. The relationship between the hysteresis loop parameters K_i and L_i and the gas content was analyzed by Gaussian fitting, and the results are shown in Figure 8(b). Notably, adsorption reaches a peak at 20.48

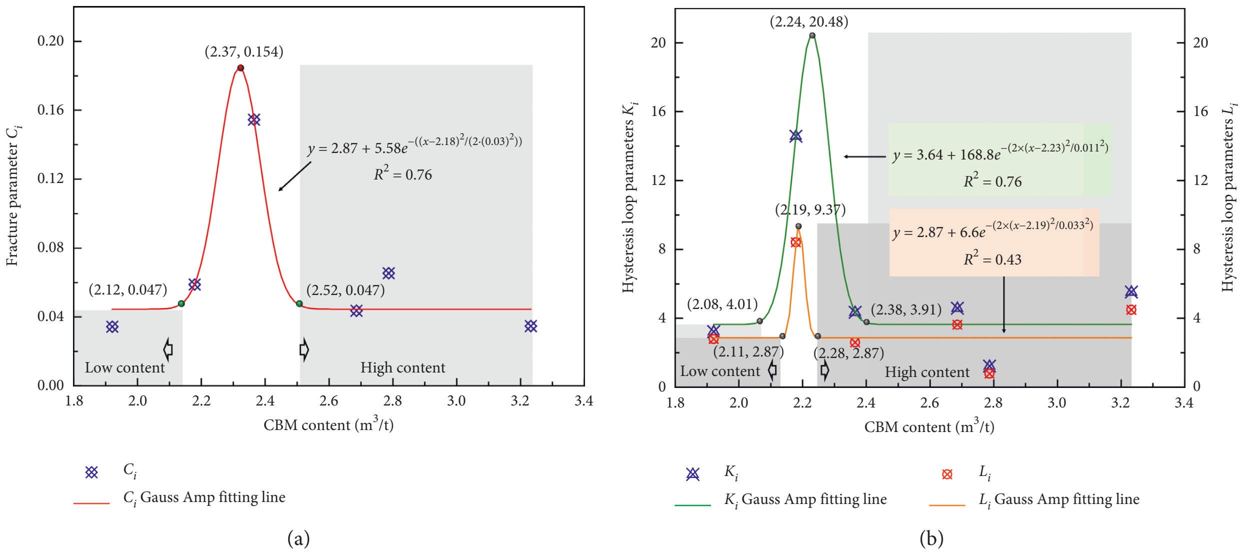

Figure 8: Analysis of the relationships of the CBM content and parameters of micropores and microfractures: (a)relations of parameter C_i and CBM content; (b) relations of adsorption, desorption parameters, and CBM content.

when the gas content is 2.24 m^3/t. L_i reaches a peak at 9.37 when the gas content is 2.19 m^3/t. The hysteresis loop parameters K_i and L_i must be sufficiently small. Therefore, the distance between the initial point and the ending point must be decreased so that the gas content remains relatively high. In conclusion, the development of microfractures inhibits gas accumulation. Specifically, the more expansive the fracture development is, the lower the gas content is. Conversely, the development of micropores is good for gas accumulation, yields small values for the hysteresis loop parameters K_i and L_i, and results in high gas contents.

4.3. Correlation Dimension for Multiparameter Calculations. The correlation dimension is a key factor used to quantify changes in chaotic time series, and correlation dimension analysis is an important branch of fractal theory. The GP algorithm uses a correlation integral to calculate the correlation values of variables and determine the regularity and degree of change. Thus, this approach reconstructs the phase space. Thresholds must be defined for different parameters. In this approach, two parameters are considered related when the difference in dimension is smaller than the threshold, and the opposite is true as well. Correlated parameters are identified and grouped in phase space. The greater the number of parameters in a group, the higher the associated correlation is. The microfracture parameter C_i, hysteresis loop parameters K_i and L_i, and gas content q_i are selected for analysis. In addition, 5 of the 103 characteristic parameters plotted in the Gaussian curve are added to the database. MATLAB 2014R software is used to analyze the relationship between the time-series correlation integral $C(r)$ and distance r in the reconstructed phase space. Then, the correlation dimensions are calculated after analyzing the time series using the delay embedding method. The correlation dimensions are used as indicators to quantitatively evaluate the effects of the microfeatures of the coal reservoir on the gas content.

The GP algorithm and delay embedding method combined with the saturation correlation dimension are used to calculate the minimum embedding dimension. Specifically, the minimum embedding dimension is expressed as $m = m_0 + 1$, when the estimated correlation dimension D_m hardly varies with an increase in the embedding dimension. Based on the relationship between correlation integral $C(r)$ and distance r in the reconstructed phase space, the slope of the nonscaling interval on the fitting line is the correlation dimension based on the least square method.

Figure 9(a) shows that the estimated correlation dimension linearly increasing when m_0 is 1, 2, 3, or 4. The value of the estimated correlation dimension becomes stable when m_0 is larger than 7. Thus, the embedding dimension is 8. Based on dividing the $\ln C(r) - \ln(r)$ curve into sections, the slope of the A-B interval defined as the correlation dimension D is 2.17, as shown in Figure 9(b).

The relationship between micropore and microfracture parameters and CBM content can be quantitatively defined by the correlation dimension. Figure 10(a) shows that the correlation dimension is 0.425 in the reconstructed phase space consisting of the microfracture parameter C_i and the CBM content q_i. The correlation dimension is 3.57 in the reconstructed phase space consisting of the microfracture parameters K_i and L_i and the CBM content q_i as shown in Figure 10(b). The results show that the hysteresis loop parameters K_i and L_i have a dramatic impact on the CBM content q_i. The calculation results provide a quantitative assessment of the relationships among tectonic structures, the microfeatures of the coal reservoir, and the CBM content.

5. Conclusion

(1) The microfracture characteristics of coal samples can be quantitatively described based on the Kirsch recognition algorithm and X-ray images.

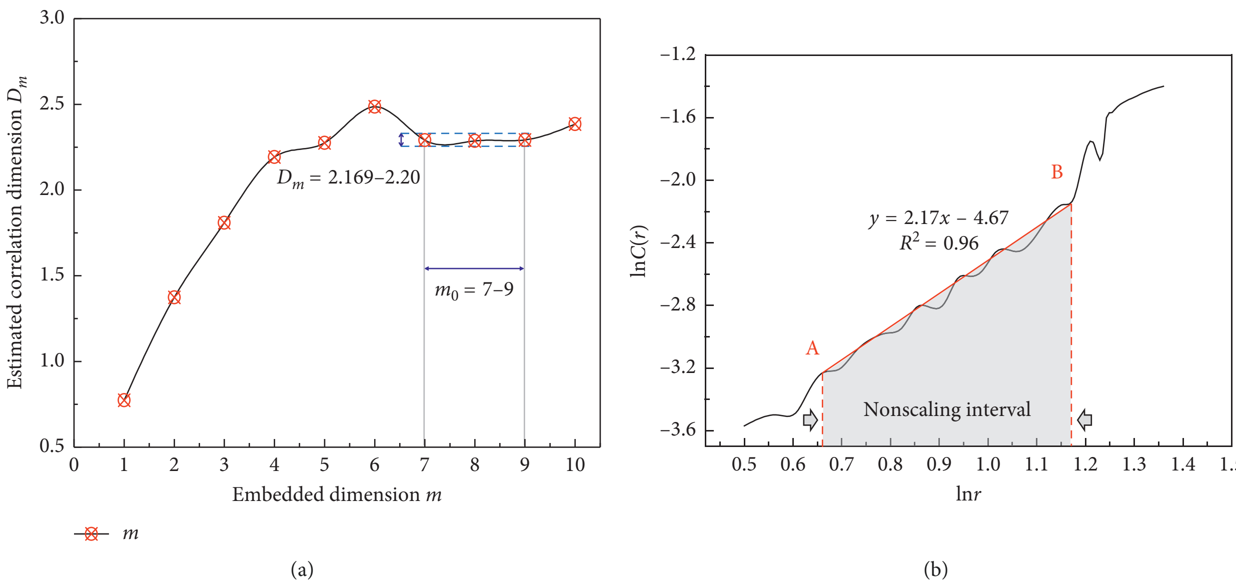

FIGURE 9: Correlation dimension in the reconstructed phase space: (a) relationship between the reconstructed phase space and embedding dimension; (b) $\ln C(r)$ and $\ln r$ curve in log-log coordinates.

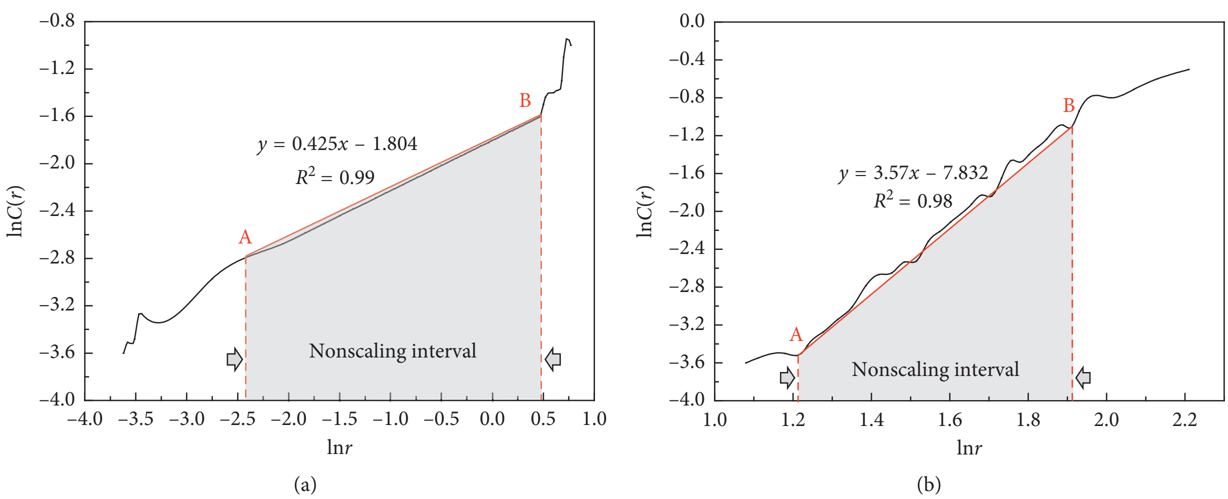

FIGURE 10: Correlation dimension of micropore and microfracture parameters: (a) $\ln C(r)$ and $\ln r$ curve in log-log coordinates in the reconstructed phase space of C_i and q_i; (b) $\ln C(r)$ and $\ln r$ curve in log-log coordinates in the reconstructed phase space of K_i, L_i, and q_i.

Additionally, C_i is presented based on microfracture features, and the results indicate that the microfracture degree of coal samples obviously differs in tectonic zones.

(2) The N_2 adsorption/desorption isotherms of coal samples were defined as three types associated with syncline, anticline, and fault areas. Notably, the pore size and pore distribution of coal specimens from fault areas were observably different than those of coal samples from syncline and anticline areas. These results suggest that the pore structure system evolves with tectonic stress.

(3) The correlation dimension was calculated with the GP algorithm. The relationships among the experimental time series of the microfracture parameters of coal samples from different tectonic zones were analyzed. Additionally, the hysteresis loop parameters of adsorption/desorption isotherms and the CBM content were considered. The micropore and microfracture characteristics of coal samples around different tectonic zones exhibited a nonlinear relationship with the CBM content, and this relation could be quantitatively defined as a correlation dimension.

Data Availability

The data used to support the findings of this study are included within the article.

Conflicts of Interest

The authors declare that they have no conflicts of interest.

Acknowledgments

This work was supported by the Open Project of Key Laboratory of Coal Resources Exploration and Comprehensive Utilization, Ministry of Land and Resources (Grant no. KF 2018-1).

Supplementary Materials

Adsorption-desorption isotherms were drawn based on liquid nitrogen experiment data, which is shown in supplementary materials. (*Supplementary Materials*)

References

[1] T. A. Moore, "Coalbed methane: a review," *International Journal of Coal Geology*, vol. 101, pp. 36–81, 2012.

[2] S. Chen, D. Tang, S. Tao et al., "In-situ stress measurements and stress distribution characteristics of coal reservoirs in major coalfields in China: implication for coalbed methane (CBM) development," *International Journal of Coal Geology*, vol. 182, pp. 66–84, 2017.

[3] D. M. Liu, Z. T. Li, and Y. D. Cai, "Study progress on pore-crack heterogeneity and geological influence factors of coal reservoir," *Coal Science and Technology*, vol. 43, pp. 10–15, 2015.

[4] W. Jiang, C. F. Wu, K. Zhao, and C. C. Liang, "Study on pore characteristics of coal reservoir and CBM recoverability in multiple coal seam blocks," *Coal Science and Technology*, vol. 43, pp. 135–139, 2015.

[5] B. Nie, X. Liu, L. Yang, J. Meng, and X. Li, "Pore structure characterization of different rank coals using gas adsorption and scanning electron microscopy," *Fuel*, vol. 158, pp. 908–917, 2015.

[6] X. Sun, P. Yang, Y. Xiang, X. Si, and D. Liu, "Across-fault distributions of radon concentrations in soil gas for different tectonic environments," *Geosciences Journal*, vol. 22, pp. 227–239, 2018.

[7] Y. Bao, C. Wei, and B. Neupane, "Generation and accumulation characteristics of mixed coalbed methane controlled by tectonic evolution in Liulin CBM field, eastern Ordos Basin, China," *Journal of Natural Gas Science and Engineering*, vol. 28, pp. 262–270, 2016.

[8] W. Ju, J. Wang, H. Fang, Y. Gong, and S. Zhang, "Paleostress reconstructions and stress regimes in the Nanchuan region of Sichuan Basin, South China: implications for hydrocarbon exploration," *Geosciences Journal*, vol. 21, pp. 553–564, 2017.

[9] A. M. M. Bustin and R. M. Bustin, "Total gas-in-place, gas composition and reservoir properties of coal of the Mannville coal measures, Central Alberta," *International Journal of Coal Geology*, vol. 153, pp. 127–143, 2016.

[10] J. J. Fan, Y. W. Ju, Q. L. Hou, J. Q. Tan, and M. M. Wei, "Pore structure characteristics of different metamorphic-deformed coal reservoirs and its restriction on recovery of coalbed methane," *Earth Science Frontiers*, vol. 17, pp. 325–335, 2010.

[11] S. Li, D. Tang, H. Xu, and Z. Yang, "Advanced characterization of physical properties of coals with different coal structures by nuclear magnetic resonance and X-ray computed tomography," *Computers & Geosciences*, vol. 48, pp. 220–227, 2012.

[12] G. Z. Deng and R. Zheng, "Micropore structure and fractal characteristics of low-permeabiligy coal seams," *Advances in Materials Science and Engineering*, vol. 2018, Article ID 4186280, 15 pages, 2018.

[13] Y. Yao, D. Liu, D. Tang, S. Tang, and W. Huang, "Fractal characterization of adsorption-pores of coals from North China: an investigation on CH4 adsorption capacity of coals," *International Journal of Coal Geology*, vol. 73, no. 1, pp. 27–42, 2008.

[14] W. Xing, Y. Song, Y. Zhang et al., "Adsorption isotherms and kinetic characteristics of methane on block anthracite over a wide pressure range," *Journal of Energy Chemistry*, vol. 24, no. 2, pp. 245–256, 2015.

[15] J. Pan, Q. Niu, K. Wang, X. Shi, and M. Li, "The closed pores of tectonically deformed coal studied by small-angle X-ray scattering and liquid nitrogen adsorption," *Microporous and Mesoporous Materials*, vol. 224, pp. 245–252, 2016.

[16] S. Zhou, D. Liu, Y. Cai, Y. Yao, and Z. Li, "3D characterization and quantitative evaluation of pore-fracture networks of two Chinese coals using FIB-SEM tomography," *International Journal of Coal Geology*, vol. 174, pp. 41–54, 2017.

[17] Y. B. Yao, D. M. Liu, and T. T. Yan, "Geological and hydrogeological controls on the accumulation of coalbed methane in the Weibei field, southeastern Ordos Basin," *International Journal of Coal Geology*, vol. 121, pp. 148–159, 2010.

[18] Y. Yao, D. Liu, Y. Cai, and J. Li, "Advanced characterization of pores and fractures in coals by nuclear magnetic resonance and X-ray computed tomography," *Science China Earth Sciences*, vol. 53, pp. 854–862, 2010.

[19] Y. B. Yao, D. M. Liu, W. H. Huang, D. Z. Tang, and S. H. Tang, "Research on the pore-fractures system properties of coalbed methane reservoirs and recovery in Huainan and Huaibei coal-fields," *Journal of China Coal Society*, vol. 2, pp. 163–168, 2006.

[20] S. Mazumder, K.-H. A. A. Wolf, K. Elewaut, and R. Ephraim, "Application of X-ray computed tomography for analyzing cleat spacing and cleat aperture in coal samples," *International Journal of Coal Geology*, vol. 68, pp. 205–222, 2006.

[21] X. F. Kong, J. Q. Guo, and T. H. Kang, "Change of pore-fracture structure of anthracite modified by electrochemical treatment using Micro-CT," *Advances in Materials Science and Engineering*, vol. 2018, Article ID 2651424, 9 pages, 2018.

[22] W. Lv, H. Y. Wang, Z. A. Yao, and L. Li, "GP predicate algorithm based on the improved computing of embedding dimension and time delay," *Computer Science*, vol. 36, pp. 187–190, 2009.

[23] S. M. Wang and Y. P. Zhang, "Study on the formation, evolution and coal·accumulating regularity of the Jurassic Ordos Basin," *Earth Science Frontiers*, vol. S1, pp. 147–155, 1999.

[24] H. T. Li and Z. F. Lv, "Trend surface analysis of the control of paleotectonics to coal accumulation of Yanan formation in Ordos Basin," *Coal Geology and Exploration*, vol. 5, pp. 7–11, 1996.

[25] Z. N. Ye, E. K. Hou, Z. H. Duan, D. He, and Y. Pan, "Prediction for gas emission quantity of the working face in Guojiahe Coal Mine," *Journal of Xi'an University of Science and Technology*, vol. 37, pp. 57–62, 2017.

[26] H. P. Xie, F. Gao, and Y. Ju, "Research and development of rock mechanics in deep ground engineering," *Chinese Journal*

of Rock Mechanics and Engineering, vol. 34, pp. 2161–2178, 2015.

[27] V. Rasouli and A. Hosseinian, "Correlations developed for estimation of hydraulic parameters of rough fractures through the simulation of JRC flow channels," *Rock Mechanics and Rock Engineering*, vol. 44, no. 4, pp. 447–461, 2011.

[28] A. Chahardehi and F. P. Brennan, "A novel weight function for RMS stress intensity factor determination in surface cracks," *Engineering Fracture Mechanics*, vol. 77, no. 2, pp. 367–373, 2010.

[29] L. Chen, E. Wang, J. Ou, and J. Fu, "Coal and gas outburst hazards and factors of the No. B-1 Coalbed, Henan, China," *Geosciences Journal*, vol. 22, no. 1, pp. 171–182, 2017.

[30] P. Chen and X. Y. Tang, "The research on the adsorption of nitrogen in low temperature and micro-pore properties in coal," *Journal of China Coal Society*, vol. 26, pp. 552–556, 2001.

[31] J. Busse, J. R. de Dreuzy, S. Galindo Torres, D. Bringemeier, and A. Scheuermann, "Image processing based characterisation of coal cleat networks," *International Journal of Coal Geology*, vol. 169, pp. 1–21, 2017.

[32] G. Z. Li, H. Y. Wang, L. X. Wu, and H. L. Liu, "Theory of syncline-controlled coalbed methane," *Natural Gas Industry*, vol. 25, pp. 26–28, 2005.

[33] Y. Li, S. Xie, J. Zhao, C. Liu, and X. Xie, "Improved GP algorithm for the analysis of sleep stages based on grey model," *ScienceAsia*, vol. 43, no. 5, pp. 312–318, 2017.

[34] S. Zhang, S. Tang, Z. Qian, Z. Pan, and Q. Guo, "Evaluation of geological features for deep coalbed methane reservoirs in the Dacheng Salient, Jizhong depression, China," *International Journal of Coal Geology*, vol. 133, pp. 60–71, 2014.

[35] J. Liu, C. J. Spiers, C. J. Peach, and S. Vidal-Gilbert, "Effect of lithostatic stress on methane sorption by coal: theory vs. experiment and implications for predicting in-situ coalbed methane content," *International Journal of Coal Geology*, vol. 167, pp. 48–64, 2016.

[36] Y.-M. Kim, H.-C. Jang, and J.-H. Lee, "Application of probabilistic approach to evaluate coalbed methane resources using geological data of coal basin in Indonesia," *Geosciences Journal*, vol. 20, no. 2, pp. 229–238, 2015.

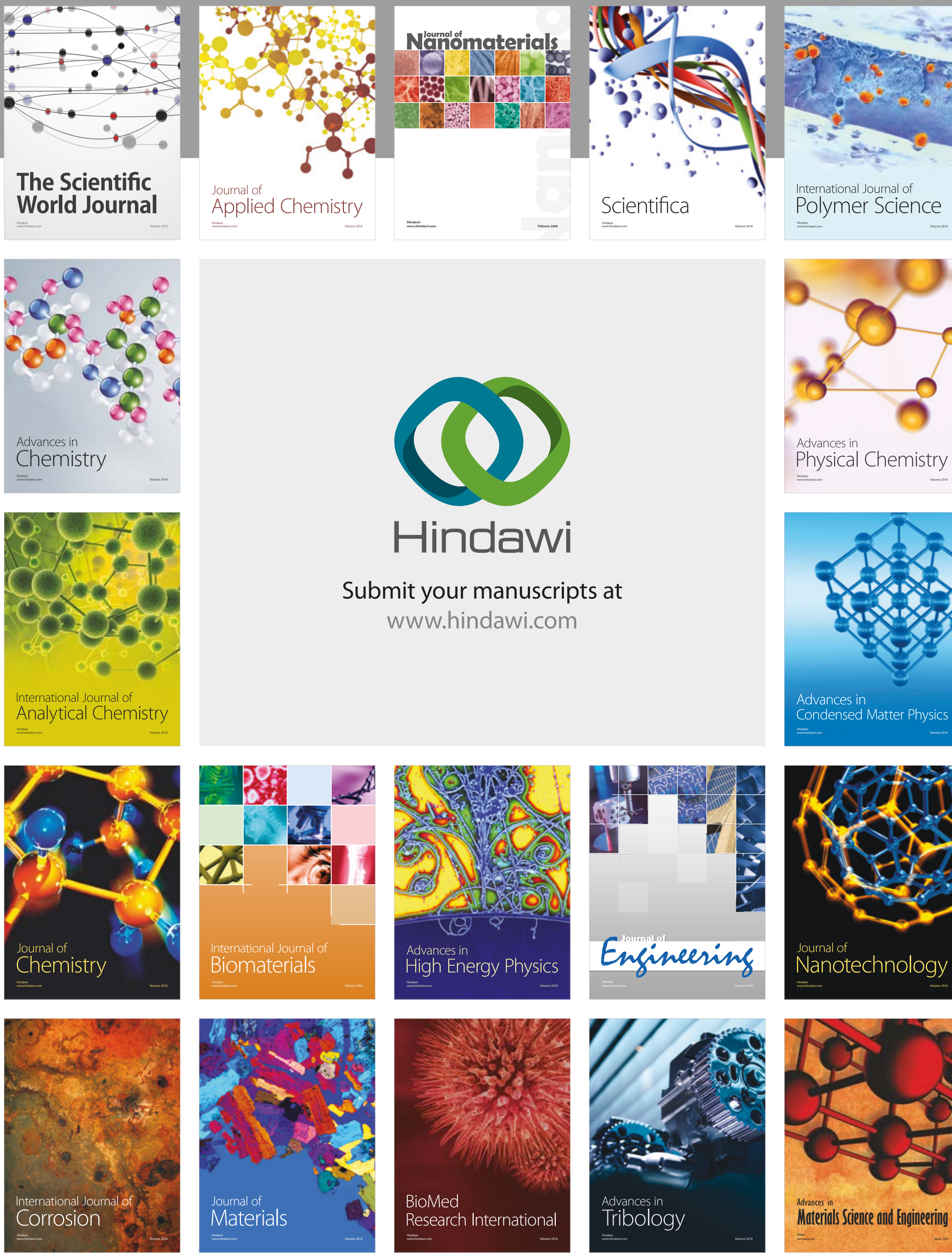
The Scientific World Journal
Journal of Applied Chemistry
Journal of Nanomaterials
Scientifica
International Journal of Polymer Science
Advances in Chemistry
Hindawi
Submit your manuscripts at
www.hindawi.com
Advances in Physical Chemistry
International Journal of Analytical Chemistry
Advances in Condensed Matter Physics
Journal of Chemistry
International Journal of Biomaterials
Advances in High Energy Physics
Journal of Engineering
Journal of Nanotechnology
International Journal of Corrosion
Journal of Materials
BioMed Research International
Advances in Tribology
Advances in Materials Science and Engineering